

Denoising Multi- β VAE: Representation Learning for Disentanglement and Generation

Anshuk Uppal*
Technical University of Denmark,
Copenhagen, Denmark
ansup@dtu.dk

Yuhta Takida
Sony AI
Tokyo, Japan

Chieh-Hsin Lai
Sony AI
Tokyo, Japan

Yuki Mitsufuji
Sony AI & Sony Group Corporation
New York, USA

Abstract

Disentangled and interpretable latent representations in generative models typically come at the cost of generation quality. The β -VAE framework introduces a hyperparameter β to balance disentanglement and reconstruction quality, where setting $\beta > 1$ introduces an information bottleneck that favors disentanglement over sharp, accurate reconstructions. To address this trade-off, we propose a novel generative modeling framework that leverages a range of β values to learn multiple corresponding latent representations. First, we obtain a slew of representations by training a single variational autoencoder (VAE), with a new loss function that controls the information retained in each latent representation such that the higher β value prioritize disentanglement over reconstruction fidelity. We then, introduce a non-linear diffusion model that smoothly transitions latent representations corresponding to different β values. This model denoises towards less disentangled and more informative representations, ultimately leading to (almost) lossless representations, enabling sharp reconstructions. Furthermore, our model supports sample generation without input images, functioning as a standalone generative model. We evaluate our framework in terms of both disentanglement and generation quality. Additionally, we observe smooth transitions in the latent spaces with respect to changes in β , facilitating consistent manipulation of generated outputs.

1 Introduction

Today, numerous advanced latent generative models are capable of producing hyperrealistic images, providing end users with a broad array of options. Current advancements in state-of-the-art generative models focus primarily on qualitative improvements in generated outputs, with recent research emphasizing the study and analysis of training dynamics to enhance generation quality (Karras et al., 2022, 2024; Hoogeboom et al., 2023, 2024). Consequently, progress in generative modeling has largely shifted focus from learning and evaluating a model’s latent representations to refining the generation process itself. However, research on deep latent generative models (Kingma et al., 2013; Radford et al., 2015) and unsupervised representation learning has shown that purposefully learned representations not only enhance generative performance but also offer practical advantages such as attribute and object changes (Wu et al., 2023).

*Work done during an internship at Sony AI.

Previous generative modeling approaches aimed at learning disentangled and interpretable latent representations have often trailed behind in generation quality. β -VAE is a fundamental method for learning such representations, based on the variational autoencoder (VAE) framework (Kingma et al., 2013). Higgins et al. (2016) modified the VAE objective by introducing a hyperparameter β , where setting $\beta = 1$ recovers the original objective function. This β parameter governs the degree of disentanglement, balancing it against reconstruction and generation quality. A larger β value imposes stronger regularization on the latent space, empirically shown to promote disentanglement, while a smaller β prioritizes reconstruction accuracy but does not encourage disentanglement. Although β -VAE has been extensively studied (H. Kim et al., 2018; Chen et al., 2018; Shao et al., 2020; Dewangan et al., 2022), overcoming this challenging trade-off in general models remains difficult and has only been addressed by a few works (Ren et al., 2022; Yang et al., 2023; Wang et al., 2023a).

Inspired by β -VAEs, we aim to promote disentangled representation learning within modern generative models. To this end, we propose a novel generative modeling framework. Our model consists of two main components, trained in a two-stage manner. First, we train a *single* VAE that learns a spectrum of latent representations by varying the parameter β , which controls disentanglement through regularization. This VAE comprises an encoder and a decoder, each conditioned on β . However, this VAE still faces the trade-off issue: disentangled latent representations with larger β lose information about the original input, leading to blurred reconstructions similar to those of a standard β -VAE. To address this, we introduce a novel non-linear diffusion model that denoises the latent variable at a given β back to an (ideally) non-lossy latent space corresponding to $\beta = 0$. This allows us to generate sharp, non-blurred images by decoding the denoised latent variable (see Fig. 1).

In our experiments, we evaluate our model in terms of both disentanglement and generation quality. For disentanglement, we demonstrate that our model effectively achieves this purpose while maintaining generation performance, by following a well-established benchmark using CelebA (Yang et al., 2023). Additionally, we benchmark our approach on well-known toy datasets (Locatello et al., 2019; Khruikov et al., 2021). Furthermore, we test our model’s capability as a standalone generative model on widely-used image datasets both qualitatively and quantitatively. We also show that the set of learned latent spaces is smooth with respect to β , which is essential for consistent manipulation.

Our contributions are briefly listed as follows.

- We propose a generative modeling framework that leverages multiple levels of latent representations, ranging from fully-informed to fully-disentangled, by extending β -VAE with a range of β values, along with a novel model design and objective function.
- We propose a novel non-linear diffusion model that connects latent spaces corresponding to different β values. By combining the VAE and the diffusion model, our approach enables both disentanglement and high-quality generation in principle.
- We empirically demonstrate that our model effectively balances disentanglement and image quality, achieving a superior trade-off compared to existing methods with the same motivation. Our approach attains disentanglement performance on par with disentanglement-focused baselines while generating high-quality images comparable to state-of-the-art generative models.

2 Overview of β -VAE

We begin with the formulation of a vanilla VAE (Kingma et al., 2013). Suppose we have a dataset $\mathcal{D} = \{\mathbf{x}_i\}_{i=1}^M$, where $\mathbf{x}_i \in \mathbb{R}^D$ for $i = \{1, \dots, M\}$. We denote the empirical distribution defined by \mathcal{D} as $p_{\mathcal{D}}(\mathbf{x})$. A VAE aims to uncover a reduced set of latent factors that give rise to this dataset.

Specifically, a latent variable $\mathbf{z} \in \mathbb{R}^d$ ($d < D$) is introduced, with its prior distribution set as $p(\mathbf{z}) = \mathcal{N}(\mathbf{0}, \mathbf{I}_d)$. Data samples are generated by first sampling $\mathbf{z} \sim p(\mathbf{z})$ and then decoding it using a probabilistic decoder, denoted as $p_{\theta}(\mathbf{x}|\mathbf{z})$. The decoder is commonly parameterized by a conditional isotropic Gaussian as $p_{\theta}(\mathbf{x}|\mathbf{z}) = \mathcal{N}(\mathbf{x}|g_{\theta}(\mathbf{z}), s^2 \mathbf{I}_D)$ with a non-negative scalar s^2 and a function $g_{\theta} : \mathbb{R}^d \rightarrow \mathbb{R}^D$. We then wish to maximize the marginal log-likelihood $\mathbb{E}_{p_{\mathcal{D}}(\mathbf{x})} [\log p_{\theta}(\mathbf{x})]$, where $p_{\theta}(\mathbf{x}) = \mathbb{E}_{p(\mathbf{z})} [p_{\theta}(\mathbf{x}|\mathbf{z})]$. However, this maximization is not tractable. Therefore, in the VAE framework, a surrogate objective function called the evidence lower bound (ELBO) is maximized instead, formulated as

$$\log p_{\theta}(\mathbf{x}) \geq \mathbb{E}_{q_{\phi}(\mathbf{z}|\mathbf{x})} [\log p_{\theta}(\mathbf{x}|\mathbf{z})] - \text{D}_{\text{KL}}(q_{\phi}(\mathbf{z}|\mathbf{x})||p(\mathbf{z})), \quad (1)$$

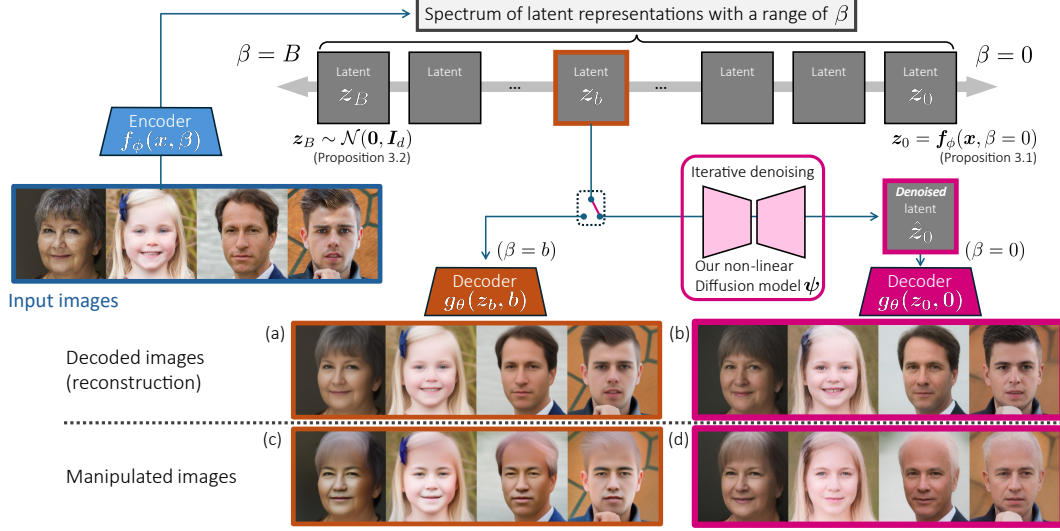


Figure 1: **Our framework for achieving both disentanglement and generation.** Our approach embeds β values as time conditioning in our newly designed nonlinear diffusion model enabling both effective disentanglement and high-quality generation. (a-b) Directly decoding z_b at non-zero b results in blurred images; however, applying the denoiser before decoding yields clear images. (c-d) The denoiser also improves the quality of manipulated images. By using the same direction in the latent space for these manipulations, we achieve consistent changes in age across different ground truth images. This demonstrates that our model produces a disentangled and easily controllable latent space. More examples of attribute changes can be found in Appendix D.5.

where $q_\phi(z|x)$ is a variational distribution used to approximate the posterior distribution $p_\theta(z|x)$, a.k.a., the encoder. A common way to model this distribution is using a conditional Gaussian as $q_\phi(z|x) = \mathcal{N}(z|f_\phi(x), \text{diag}(\sigma_\phi(x)))$, with functions $f_\phi: \mathbb{R}^D \rightarrow \mathbb{R}^d$ and $\sigma_\phi: \mathbb{R}^D \rightarrow \mathbb{R}_{\geq 0}^d$.

Through the maximization of Eq. (1), the encoder learns to recover latent generative factors from the dataset, while the decoder attempts to reconstruct x from z as accurately as possible. In other words, the encoder and decoder are trained to compress the data without information loss, effectively becoming stochastic inverses of each other. The β -VAE (Higgins et al., 2016) is a variant of the above model that employs the following modified objective function: $\mathbb{E}_{q_\phi(z|x)} [\log p_\theta(x|z)] - \beta \text{D}_{\text{KL}}(q_\phi(z|x)||p(z))$, where the *regularization term* in Eq. (1) is scaled by a hyperparameter β .

The choice of β creates a trade-off between the reconstruction quality and disentanglement of the latent representation. Previous works have established that increasing the contribution of the *regularization term*, i.e., setting $\beta > 1$, not only promotes independence among latent dimensions but also facilitates the learning of interpretable generative factors (please refer to Appendix A for this literature review). On the other hand, a downside to increasing regularization is the loss of information. When the variational approximation approaches the prior according to the KL term, all encodings $q_\phi(z|x)$ begin to collapse to the prior, resulting in a lack of distinct information about individual data points, which hampers accurate reconstruction. This indicates that setting the value of β is non-trivial due to the precarious balance between desirable disentanglement and undesirable loss of information. Even with a suitable parameter β for disentangled representation, reconstructed samples may still be blurred due to the loss of information.

In the following sections, we propose our solutions to two critical issues:

1. **Problem 1:** Choosing the optimal regularization coefficient (β) is nontrivial and requires multiple training runs. Our solution to this issue is detailed in Section 3.
2. **Problem 2:** Achieving both generation quality and controllability is challenging, as the regularization used for learning disentangled representations often degrades reconstruction and sample quality. Our solution to this issue is detailed in Section 4

3 Multi- β Representation Learning

To overcome the severe trade-off between reconstruction accuracy and the disentanglement of latent representation in existing VAE variants, we propose multi- β latent representation learning. First, we extend β -VAE by treating β as a variable rather than a hyperparameter in Section 3.1. Using a monotonic property of multi- β latent space presented in Section 3.2, a subsequently learned diffusion model allows us to move across latent spaces corresponding to different β (see Section 4).

3.1 Conditional Multi-level β -VAE

Here we extend the β -VAE to incorporate β as a variable within a range of values. In our setup, unlike the typical β -VAE, β lies in $[0, B]$ instead of being fixed, and it scales the reconstruction and regularization terms with weights of $(B - \beta)$ and β , respectively (see Eq. (4)). This approach allows us to achieve a full spectrum of the weighting, encompassing both the reconstruction-only and regularization-only objectives as extreme cases with $\beta = 0$ and B , respectively. We expect that larger values of β result in more disentangled latent representations, while smaller values will yield higher fidelity in the reconstructed samples. We assume that each value of β has its latent space, which is denoted as Z_β . In our VAE, the decoder and encoder for a given β are designed as follows:

$$p_\theta(\mathbf{x}|\mathbf{z}_\beta; \beta) = \mathcal{N}(\mathbf{x}|\mathbf{g}_\theta(\mathbf{z}_\beta, \beta), s_\beta^2 \mathbf{I}) \quad (2)$$

$$q_\phi(\mathbf{z}_\beta|\mathbf{x}; \beta) = \mathcal{N}(\mathbf{z}_\beta|\mathbf{f}_\phi(\mathbf{x}, \beta), \sigma_\beta^2 \mathbf{I}), \quad (3)$$

where $s_\beta^2 \in \mathbb{R}_{\geq 0}$, $\sigma_\beta^2 \in \mathbb{R}_{\geq 0}$, θ and ϕ represent the parameters for the decoder and encoder, respectively. Both the encoder and the decoder depend on β , which induces different latent spaces. Additionally, the conditional covariance matrices in both the data and latent spaces are modeled as learnable isotropic matrices that depend solely on β .

Under this model setup, we propose a novel objective function based on a rescaled ELBO as $\mathcal{L} = \mathbb{E}_\beta \mathcal{L}_\beta$, where

$$\mathcal{L}_\beta = \mathbb{E}_{p_{\mathcal{D}}(\mathbf{x})} \left[(B - \beta) \mathbb{E}_{q_\phi(\mathbf{z}_\beta|\mathbf{x})} [\log p_\theta(\mathbf{x}|\mathbf{z}_\beta)] - \beta \text{D}_{\text{KL}}(q_\phi(\mathbf{z}_\beta|\mathbf{x})||p(\mathbf{z})) \right], \quad (4)$$

and we sample β from a prior distribution to train the VAE across multiple β values. Notably, \mathcal{L}_β when $B = 1$, with $\beta = 0$ and 0.5 , corresponds to the objective functions for a plain autoencoder and a VAE, respectively, without considering the scaling factors². Algorithm 1 contains the training algorithm for this augmented β -VAE.

3.2 Controlling Information Loss with β

As outlined in the previous section, our objective function (4) facilitates a smooth interpolation and extrapolation between the objectives of an autoencoder and a VAE. Specifically, the parameter β modulates the degree of information retention in the latent spaces. To elucidate this mechanism, we present a simplified analysis of our novel objective function (4) in the case of $B = 1$. We anticipate that setting $\beta > 0.5$ encourages disentanglement within the latent space Z_β , albeit at the cost of information essential for accurate reconstruction. Conversely, choosing $\beta < 0.5$ enhances reconstruction fidelity but compromises the disentanglement of representations.

A smaller β value places greater emphasis on the reconstruction term, resulting in a reduced latent variance σ_β^2 . In the extreme case, setting $\beta = 0$ theoretically results in perfect reconstruction with $\sigma_0^2 = 0$, as demonstrated in the following proposition. We defer the proofs to Appendix B.

Proposition 3.1. *Under certain regularity conditions, the global optimum of \mathcal{L}_0 is achieved when $\sigma_0^2 = 0$.*

In contrast, increasing β towards 1 enhances regularization, which encourages disentanglement of the latent representation. In the extreme case, when $\beta = 1$, the objective function (4) reduces to the KL regularization term, causing $q_\phi(\mathbf{z}|\mathbf{x}; \beta = 1)$ collapse to the prior distribution $p(\mathbf{z})$. Consequently, the latent space, i.e., Z_1 , no longer retains any information about the input \mathbf{x} , as demonstrated in the following proposition.

²Our β is different from that of the typical β -VAE in the relationship between β values and their respective models.

Proposition 3.2. *The mutual information between the input and the reconstructed samples produced by the VAE becomes zero as $D_{\text{KL}}(q_\phi(\mathbf{z}|\mathbf{x}; \beta = 1) \parallel p(\mathbf{z}))$ converges to zero. It holds for any decoder function $g_\theta(\cdot, \beta = 1)$.*

The gradual loss of information in the latent space with β is also characterised by a gradual increase in the variance of latent representations such that $\sigma_\beta < \sigma_{\beta'}$ for $0 \leq \beta < \beta' \leq 1$, which is also observed in previous studies (Takida et al., 2022).

In summary, our multi-level β -VAE is equipped to learn a slew of latent representations which due to Eq. (4), capture major axes of variation present across the dataset by down-weighting accurate reconstructions. This does not mitigate Problem 2. To this end, we purposely combine the model Eq. (3) and Eq. (4) so that learnt σ_β parallel a typical noising process in diffusion models ($\beta \equiv t$). When trained well, diffusion models can capture the target distribution and sample realistic data by repeated denoising. However, due to the involvement of an encoder that specifies the mean $\mathbf{f}_\phi(\mathbf{x}, \beta)$ at all $\beta \in [0, 1]$ in the latent space, our noising process diverges from the commonly used linear inference/noising process. We detail our formulation of non-linear denoising diffusion in the next section.

4 Reversing the Information Loss

Increasing regularization enhances representation learning but negatively affects sample and reconstruction quality. At higher β values, the reconstructions tend to collapse into an ‘‘averaged’’ image, a phenomenon also noted by Collins et al. (2022). To address Problem 2, we propose reversing information loss by training a denoising model based on a diffusion process. First, we review the standard diffusion model in Section 4.1 and its nonlinear extension in Section 4.2. In this approach, the time-varying mean is governed by the encoder (\mathbf{f}_ϕ), with noise conditioning parameterized by β or equivalently by time t .

4.1 Primer on Diffusion Models

We start with a brief primer on the vanilla diffusion models with a linear diffusion process. Diffusion models consist of a fixed hierarchical encoding process, known as the forward or noising process, and a decoding process for generation. In the encoding stage, incremental noise is gradually added to the data, transforming it into a Gaussian noise:

$$q(\mathbf{z}_t|\mathbf{x}; t) := \mathcal{N}(\mathbf{z}_t|\mathbf{x}, \sigma_t^2 \mathbf{I}_d), \quad (5)$$

where $t \in [0, T]$, $\tau > 0$ is a small constant, and $\sigma_t > 0$ is a predefined noise schedule that increases with t . Next, the Markovian forward distributions are derived as

$$q(\mathbf{z}_t|\mathbf{z}_{t-\tau}) = \mathcal{N}(\mathbf{z}_t|\mathbf{z}_{t-\tau}, \sigma_{t|t-\tau}^2 \mathbf{I}_d), \quad (6)$$

where $\sigma_{t|t-\tau}^2 = \sigma_t^2 - \sigma_{t-\tau}^2$. A tractable reverse decoding process is obtained via Bayes’ rule as

$$q(\mathbf{z}_{t-\tau}|\mathbf{z}_t, \mathbf{x}) = \mathcal{N}(\mathbf{z}_{t-\tau}|\tilde{\boldsymbol{\mu}}_t(\mathbf{z}_t, \mathbf{x}), \tilde{\sigma}_t^2 \mathbf{I}_d), \quad (7)$$

$$\text{where } \tilde{\sigma}_t^2 = \frac{\sigma_{t|t-\tau}^2 \sigma_{t-\tau}^2}{\sigma_t^2} \text{ and } \tilde{\boldsymbol{\mu}}_t(\mathbf{z}_t, \mathbf{x}) = \frac{\sigma_{t-\tau}^2}{\sigma_t^2} \mathbf{z}_t + \frac{\sigma_{t|t-\tau}^2}{\sigma_t^2} \mathbf{x}. \quad (8)$$

Diffusion models are trained to match the generative reverse conditional distributions in Eq. (7), and are generally parameterized as

$$p_\psi(\mathbf{z}_{t-\tau}|\mathbf{z}_t) := \mathcal{N}(\mathbf{z}_{t-\tau}|\boldsymbol{\mu}_\psi(\mathbf{z}_t, t), \sigma_r^2(t) \mathbf{I}_d), \quad (9)$$

$$\text{where } \boldsymbol{\mu}_\psi(\mathbf{z}_t, t) := \frac{\sigma_{t-\tau}^2}{\sigma_t^2} \mathbf{z}_t + \frac{\sigma_{t|t-\tau}^2}{\sigma_t^2} \hat{\mathbf{x}}_\psi(\mathbf{z}_t, t). \quad (10)$$

$\hat{\mathbf{x}}_\psi$ is known as the *denoiser*. Equivalently, we parametrize it as a noise prediction model $\hat{\epsilon}_\psi$, where $\hat{\mathbf{x}}_\psi(\mathbf{z}_t, t) = \mathbf{z}_t - \sigma_t \hat{\epsilon}_\psi(\mathbf{z}_t, t)$. The loss function of a diffusion model is derived using an ELBO (by extending Eq. (1) with time hierarchy), aiming to match the conditional distributions in Eq. (7) and Eq. (9) over all $t \in [0, T]$ using the KL divergence. This loss boils down to a simple regression loss:

$$\min_{\psi} \mathbb{E}_{t, \mathbf{x}} \mathbb{E}_{\mathbf{z}_t|\mathbf{x}} \left[\frac{1}{2\tilde{\sigma}_t^2} \|\boldsymbol{\mu}_\psi(\mathbf{z}_t, t) - \tilde{\boldsymbol{\mu}}_t(\mathbf{z}_t, \mathbf{x})\|_2^2 \right]. \quad (11)$$

By discretizing the time such that $t \in \{iT/N\}_{i=0}^N$ for the iterative decoding, we obtain a hierarchical generator:

$$p_\psi(\mathbf{x}) = \int_{\mathbf{z}} p(\mathbf{x}|\mathbf{z}_0)p(\mathbf{z}_B) \prod_{i=1}^N p_\psi\left(\mathbf{z}_{\frac{(i-1)T}{N}} \middle| \mathbf{z}_{\frac{iT}{N}}\right), \quad (12)$$

where $p(\mathbf{z}_T) = \mathcal{N}(\mathbf{z}_T|0, \mathbf{I}_d)$.

4.2 Non-linear Diffusion in Latent Space

We propose a non-linear (in \mathbf{x}) denoising diffusion for use in our model. In this subsection, time variables t (and T) are interchangeable with β (and B), as they represent the same concept. We hinted in Section 3.2 that our non-linear diffusion process is prescribed by the β - or time-dependent encoder. Formally, the distribution of \mathbf{z}_t for given \mathbf{x} is

$$q_\phi(\mathbf{z}_t|\mathbf{x}; t) = \mathcal{N}(\mathbf{z}_t|\mathbf{f}_\phi(\mathbf{x}, t), \sigma_t^2 \mathbf{I}_d). \quad (13)$$

This expression is just an adaptation of Eq. (3) with $\beta = t$, and is more general than Eq. (5). We propose the nonlinear Markovian encoding process as

$$q_\phi(\mathbf{z}_t|\mathbf{z}_{t-\tau}, \mathbf{x}) = \mathcal{N}(\mathbf{z}_t|\mathbf{z}_{t-\tau} + \mathbf{f}_\phi(\mathbf{x}, t) - \mathbf{f}_\phi(\mathbf{x}, t-\tau), \sigma_{t|t-\tau}^2). \quad (14)$$

This form closely resembles Eq. (6). Following the development in Section 4.1, we now define the reverse of Eq. (14) as:

$$q_\phi(\mathbf{z}_{t-\tau}|\mathbf{z}_t, \mathbf{x}) = \mathcal{N}(\mathbf{z}_{t-\tau}|\tilde{\boldsymbol{\mu}}_t(\mathbf{z}_t, \mathbf{x}), \tilde{\sigma}_t^2 \mathbf{I}_d), \quad (15)$$

$$\text{where } \tilde{\boldsymbol{\mu}}_t(\mathbf{z}_t, \mathbf{x}) = \frac{\sigma_{t-\tau}^2}{\sigma_t^2} \mathbf{z}_t + \frac{\sigma_{t|t-\tau}^2}{\sigma_t^2} \mathbf{x} + \mathbf{f}_\phi(\mathbf{x}, t-\tau) - \mathbf{f}_\phi(\mathbf{x}, t), \quad (16)$$

with $\tilde{\sigma}_t^2$ remaining the same as Eq. (8). Due to the additional \mathbf{f}_ϕ terms in this flavour of the diffusion model, $\boldsymbol{\mu}_\psi$ cannot follow the same parameterization as in Eq. (10). Instead we introduce a new approach to express the mean prediction in this case, as follows:

$$\boldsymbol{\mu}_\psi(\mathbf{z}_t, t) := \frac{\sigma_{t-\tau}^2}{\sigma_t^2} \mathbf{z}_t + \frac{\sigma_{t|t-\tau}^2}{\sigma_t^2} \hat{\mathbf{x}}_\psi(\mathbf{z}_t, t) + \hat{\Delta}_\psi(\mathbf{z}_t, t). \quad (17)$$

Eq. (17) introduces an extra predictor $\hat{\Delta}_\psi$ for learning the evolution of encodings with time. In practice, we train noise prediction, reparameterizing $\hat{\mathbf{x}}_\psi(\mathbf{z}_t, t)$ with $\hat{\epsilon}_\psi(\mathbf{z}_t, t)$, along with an encoding difference predictor $\hat{\Delta}_\psi(\mathbf{z}_t, t)$, which is novel to the best of our knowledge.

Following the parameterization of $\boldsymbol{\mu}_\psi$, our model training differs from standard practice in a couple of key ways. First, we do not train the noise prediction network to predict the noise added to $\mathbf{z}_0 = \mathbf{f}_\phi(\mathbf{x}, 0)$ given a sample \mathbf{z}_t . The transition from \mathbf{z}_0 to \mathbf{z}_t is non-linear due to the encoder and depends on its Jacobian, $\frac{d\mathbf{f}_\phi(\mathbf{x}, t)}{dt}$. Rather than learning an inversion of this time-varying encoding, we aim to learn the direction of the noise (ϵ_t) at each time step $t \in [0, T]$ using $\hat{\epsilon}_\psi(\mathbf{z}_t, t)$, i.e.,

$$\mathbb{E}_{t, \mathbf{x}} \mathbb{E}_{\epsilon_t} \mathbb{E}_{\mathbf{z}_t|\mathbf{x}, \epsilon_t} \left[\frac{1}{w(t)} \|\hat{\epsilon}_\psi(\mathbf{z}_t, t) - \epsilon_t\|_2^2 \right] \text{ with } \mathbf{z}_t = \mathbf{f}_\phi(\mathbf{x}, t) + \sigma_t \epsilon_t \text{ and } \epsilon_t \sim \mathcal{N}(\mathbf{0}, \mathbf{I}_d), \quad (18)$$

where $w(t)$ is a weighting function. This approach trains the model to denoise at each time step. Additionally, $\hat{\Delta}_\psi$ is necessary for sampling and is trained to predict the change in \mathbf{f}_ϕ over a small time interval τ ³. Assuming that the encoder is a smooth function, this design is based on the intuition that learning encoding differences over one time step is easier than over arbitrarily large steps.

We adjust the diffusion model's U-Net to produce two outputs, $\hat{\epsilon}_\psi(\mathbf{z}_t, t)$, $\hat{\Delta}_\psi(\mathbf{z}_t, t)$. Using these predictions, we build our DDPM (Ho et al., 2020)-inspired sampling algorithm, as shown in Algorithm 2. The actual loss function used to train this new diffusion model is defined as

$$\mathbb{E}_{t, \mathbf{x}} \mathbb{E}_{\epsilon_t} \mathbb{E}_{\mathbf{z}_t|\mathbf{x}, \epsilon_t} \left[\frac{1}{w(t)} \|\hat{\epsilon}_\psi(\mathbf{z}_t, t) - \epsilon_t(\mathbf{x}, \epsilon_t)\|_2^2 + \|\mathbf{f}_\phi(\mathbf{x}, t-\tau) - \mathbf{f}_\phi(\mathbf{x}, t) - \hat{\Delta}_\psi(\mathbf{z}_t, t)\|_2^2 \right]. \quad (19)$$

³In implementation, we set $\tau = T/N$ in the discrete time setup, learning the single time-step encoding difference for all times.

Algorithm 1: Training of our VAE

Input: Dataset \mathcal{D} , β -schedule $\{\beta_i\}_{i=1}^N$, learning rate η , number of training steps S

Output: Trained networks, ϕ , θ , and $\sigma = \{\sigma_\beta\}_{\beta \in \{\beta_i\}_{i=1}^N}$

```

for  $s = 1, 2, \dots, S$  do
1   Sample:  $\mathbf{x} \sim p_{\mathcal{D}}(\mathbf{x})$ ,  $\beta \sim \mathcal{U}([0, 1])$ ,  $\epsilon \sim \mathcal{N}(\mathbf{0}, \mathbf{I}_d)$ 
2   Generate noisy encoding:
       $\mathbf{z}_\beta = \mathbf{f}_\phi(\mathbf{x}, \beta) + \sigma_\beta \epsilon$ 
3   Compute the objective  $\mathcal{L}$  based on Eq. (4)
4   Update parameters:  $\omega \leftarrow \omega - \eta \nabla_\omega \mathcal{L}$ ,
      where  $\omega = \{\theta, \phi, \sigma\}$ 
return  $\mathbf{f}_\phi, \mathbf{g}_\theta, \sigma$ 

```

Algorithm 2: Sampling of our diffusion

Input: Trained model ϵ_ψ , total time steps N , largest time T , trained noise schedule $\sigma = \{\sigma_t\}_{t \in \{0, T/N, \dots, (N-1)T/N, T\}}$

Output: Generated sample \mathbf{z}_0

Initialize: $\mathbf{z}_T \sim \mathcal{N}(\mathbf{0}, \mathbf{I}_d)$

```

for  $t = T, (N-1)T/N \dots, T/N$  do
1   Predict noise and diff:
       $\hat{\epsilon} = \hat{\epsilon}_\psi(\mathbf{z}_t, t)$ ,  $\hat{\Delta} = \hat{\Delta}_\psi(\mathbf{z}_t, t)$ 
2   Compute mean for  $\mathbf{z}_t$ :
       $\mu_t = \mathbf{z}_t - \sigma_t \hat{\epsilon}$ 
3   Predict previous mean:
       $\mu_{t-T/N} = \mu_t - \hat{\Delta}$ 
4   Update  $\mathbf{z}_{t-T/N}$  (with  $\epsilon \sim \mathcal{N}(\mathbf{0}, \mathbf{I}_d)$ ):  $\mathbf{z}_{t-T/N} = \mu_{t-T/N} + \sigma_{t-T/N} \epsilon$ 
return  $\mathbf{z}_0$ 

```

Integrating the conditional multilevel β -VAE, as introduced in Section 3.1, with the diffusion model described in Section 4.2 is key to mitigating the disentanglement-reconstruction trade-off in our framework.

We now combine the two proposed modules from Section 3 and Section 4 into a single model, trained in two phases. In the first phase, we train the conditional multilevel β -VAE using the loss defined in Eq. (4) (Algorithm 1). After this, we train the non-linear diffusion model from Section 4.2, keeping the autoencoder parameters fixed. Additionally, depending on the dataset, we fine-tune the decoder with an adversarial loss, following Rombach et al. (2021), to enhance generation quality. Further training details are provided in Appendix C.

5 Related Works

β -VAE and its variants have been extensively studied for their distinct capabilities (Burgess et al., 2017) and wide-ranging applications in domains such as images (Higgins et al., 2016), text (Shao et al., 2020), and molecular generation (Richards et al., 2022). These models are especially valued for their interpretable latent representations, achieved through β -controlled regularization.

H. Kim et al. (2018) improved disentanglement while maintaining reconstruction quality by combining the ELBO with a total correlation term. Similarly, Chen et al. (2018) enhanced mutual information between latent variables and observed data to promote independence among latent factors. Shao et al. (2020) introduced an adaptive feedback mechanism that adjusts β during training based on KL divergence. Dewangan et al. (2022) applied a deep convolutional β -VAE for feature extraction in industrial fault diagnosis, using a variable β training protocol without conditioning the encoder and decoder on β .

Both Collins et al. (2022) and Bae et al. (2023) investigated training VAEs with multiple β values, with Bae et al. (2023) capturing the full rate-distortion curve using a hypernetwork conditioned on β , and Collins et al. (2022) focusing on particle physics applications. In contrast, our framework enables high-fidelity generation from disentangled representations (with larger β) by linking latent spaces through a novel non-linear diffusion process, along with specific adjustments to the β -conditioned VAE to optimize the latent space for diffusion.

Recently, a few methods have emerged to achieve disentanglement while preserving generation fidelity. Wang et al. (2023b) developed InfoDiffusion, a pioneering diffusion-based model that extends the Diffusion Autoencoder (DiffAE, Preechakul et al., 2022). Yang et al. (2023) introduced DisDiff, which adds encoder and decoder components to pre-trained diffusion models to maintain

generation quality, rather than training disentanglement-focused models from scratch. Ren et al. (2022) focus on building an exploration technique for pre-trained generative models for post-hoc identification of disentangled directions. Notably, in contrast to training-free methods our approach encourages disentanglement during training, assuring a more disentangled representation.

Our method falls within the model-training-based category, similar to InfoDiffusion, but it uniquely learns a spectrum of latent representations that provide a distinct advantage. Combined with the learned non-linear diffusion model, our framework enables transitions between highly disentangled and fully informed latent representations, facilitating the generation of high-fidelity outputs. Additionally, we show in Appendix D.1 (see Table 7) that finding-based methods like DisCo (Ren et al., 2022) can complement our approach, indicating potential for combined implementations.

6 Experiments

We quantitatively demonstrate that our method achieves both disentanglement and high-quality generation within a single model. We will focus on each of these aspects individually. Specifically, in Section 6.1, we examine the disentanglement of the learned latent representations. In Section 6.2, we evaluate our model’s unconditional generation performance and report standard metrics on commonly used image datasets. Additional details regarding the experiments can be found in the appendix.

6.1 Evaluating Disentanglement

6.1.1 Image Dataset

To demonstrate that our method effectively obtains disentangled representation while maintaining high generation quality, we verify our approach on an image dataset. Specifically, we follow the protocol established by Yang et al. (2023) using the CelebA dataset (Liu et al., 2015). In this setup, we calculate Total AUROC Difference (TAD, Yeats et al., 2022) and FID (Heusel et al., 2017) scores. TAD is a disentanglement metric for datasets with binary attribute labels that measures how well latent variables uniquely capture ground truth attributes. As shown in Table 1, our method achieves the best performance in both aspects compared to the baselines, including state-of-the-art methods that aim to address the significant trade-off between these two factors, such as InfoDiffusion (Wang et al., 2023b) and DisDiff (Yang et al., 2023).

Table 1: TAD and FID scores on CelebA. Our model outperforms baselines in terms both of disentanglement and generation quality.

Method	TAD (\uparrow)	FID (\downarrow)
β -VAE	0.088 ± 0.043	99.8 ± 2.4
InfoVAE	0.000 ± 0.000	77.8 ± 1.6
DiffAE	0.155 ± 0.010	22.7 ± 2.1
InfoDiffusion	0.299 ± 0.006	23.6 ± 1.3
DisDiff	0.305 ± 0.010	18.3 ± 2.1
Ours	0.378 ± 0.017	17.9 ± 1.9

6.1.2 Common Benchmark with Toy Datasets

To compare our model with baselines dedicated to disentanglement (at the expense of generation quality) such as FactorVAE (H. Kim et al., 2018), β -TCVAE (Chen et al., 2018), and InfoGAN-CR (Lin et al., 2020), we adopt the evaluation protocols of Locatello et al. (2019) and Khrulkov et al. (2021) using toy datasets: Cars3D (Reed et al., 2015), Shapes3D (H. Kim et al., 2018), and MPI3D (Gondal et al., 2019). For assessment, we use the Mutual Information Gap (MIG) (Chen et al., 2018) and the Disentanglement metric (Eastwood et al., 2018). The MIG measures how well latent dimensions respond to changes in individual generative factors, while DCI (Disentanglement, Completeness, and Informativeness) evaluates the extent to which factors are distinctly represented by individual latent dimensions, the exclusivity of each factor to a specific dimension, and the comprehensiveness of the overall representation. Table 2 shows that our model achieves disentanglement performance comparable to or surpassing that of other disentanglement models.

We also compare our approach with DisCo (Ren et al., 2022), another approach that uses contrastive learning to find the appropriate directions in the latent space of a pre-trained generative model while preserving its generative capabilities. We demonstrate the finding-based approach is complementary to our method in Appendix D.1 (see Table 7).

Table 2: **Disentanglement Metrics.** We evaluate our multi- β VAE representations through benchmarking on well-known toy datasets and comparing them to baselines that aim to learn disentangled representation. In each column, the best results are highlighted in bold, and the second-best results are underlined.

Method	Cars3D		Shapes3D		MPI3D	
	MIG \uparrow	DCI \uparrow	MIG	DCI	MIG	DCI
FactorVAE	0.128 \pm 0.036	0.160 \pm 0.020	<u>0.411</u> \pm 0.163	0.611 \pm 0.127	0.098 \pm 0.027	<u>0.246</u> \pm 0.066
β -TCVAE	0.080 \pm 0.024	0.140 \pm 0.020	0.406 \pm 0.190	<u>0.613</u> \pm 0.151	0.108 \pm 0.053	0.239 \pm 0.062
InfoGAN-CR	0.011 \pm 0.009	0.020 \pm 0.011	0.297 \pm 0.124	0.478 \pm 0.055	0.161 \pm 0.077	0.242 \pm 0.076
Ours	<u>0.117</u> \pm 0.009	<u>0.157</u> \pm 0.010	0.422 \pm 0.090	0.621 \pm 0.090	<u>0.147</u> \pm 0.035	0.253 \pm 0.043

Table 3: **Generation Quality.** We evaluate our model for unconditional image synthesis and report standard metrics, comparing them against baselines specifically designed for generation.

CelebA-HQ 256×256				FFHQ 256×256				LSUN-Bedrooms 256×256			
Method	FID \downarrow	Prec. \uparrow	Recall \uparrow	Method	FID \downarrow	Prec. \uparrow	Recall \uparrow	Method	FID \downarrow	Prec. \uparrow	Recall \uparrow
DC-VAE(Parmar et al., 2021)	15.8	-	-	ImageBART(Esser et al., 2021a)	9.57	-	-	ImageBART(Esser et al., 2021a)	5.51	-	-
VQGAN+T(Esser et al., 2021b)	10.2	-	-	U-Net GAN(Schonfeld et al., 2020)	10.9	-	-	DDPM(Ho et al., 2020)	4.9	-	-
PGGAN(Karras et al., 2018)	8.0	-	-	UDM(D. Kim et al., 2021)	5.54	-	-	UDM(D. Kim et al., 2021)	4.57	-	-
LSGM(Vahdat et al., 2021)	7.22	-	-	StyleGAN(Karras et al., 2019)	4.16	0.71	0.46	StyleGAN(Karras et al., 2019)	2.35	0.59	0.48
UDM(D. Kim et al., 2021)	7.16	-	-	ProjectedGAN(Sauer et al., 2021)	3.08	0.65	0.46	ADM(Dhariwal et al., 2021)	1.90	0.66	0.51
Ours	6.41	0.71	0.48	Ours	5.45	0.72	0.48	Ours	3.2	0.65	0.48

6.2 Evaluating Generation Quality

We demonstrate that our model can serve as a standalone generation model by evaluating its generation quality on practical image datasets, including CelebA-HQ (Karras et al., 2018), FFHQ (Karras et al., 2019), and LSUN-Bedrooms (Yu et al., 2015), at a resolution of 256×256 . For these image datasets, we evaluate our model using FID to assess image quality and precision-recall (Kynkäänniemi et al., 2019) to gauge data distribution coverage. Details of our architecture and training times are provided in Appendix C, and generated sample images are shown in Appendix D.4.

While our model is designed to learn disentangled latent representations, it is crucial that this capability does not compromise generation quality. Based on our comparative performance with generation-focused baselines in Table 3, we conclude that our model effectively generates high-quality images at this resolution across various datasets.

Lastly, we visualize generated samples from various β values in Fig. 2 to demonstrate the smoothness of our latent space spectrum in terms of β or t . We encode ground truth images to latent representations at certain β values, denoise them using our non-linear diffusion, and decode them to obtain clear images. We observe that generated images with different values of β remain consistent with each other. Another smoothness perspective, spatial smoothness of the latent spaces, is visualized in Appendix D.5.

7 Conclusion

We propose a new generative modeling framework that leverages a range of β values to learn disentangled representations and sharp generation quality, including unconditional generation. Our framework introduces two key components: (1) a multi- β VAE, producing a spectrum of latent representations that can be refined via a denoising diffusion process, and (2) a non-linear diffusion model that links latent representations for different β values. Our method offers a superior trade-off compared to existing approaches. Additionally, it achieves comparable disentanglement performance to dedicated baselines while maintaining high decoding quality and generating results on par with state-of-the-art generation models.

References

Bae, Juhan, Michael R. Zhang, Michael Ruan, Eric Wang, So Hasegawa, Jimmy Ba, and Roger Baker Grosse (2023). “Multi-Rate VAE: Train Once, Get the Full Rate-Distortion Curve”. In: *The Eleventh International Conference on Learning Representations*.

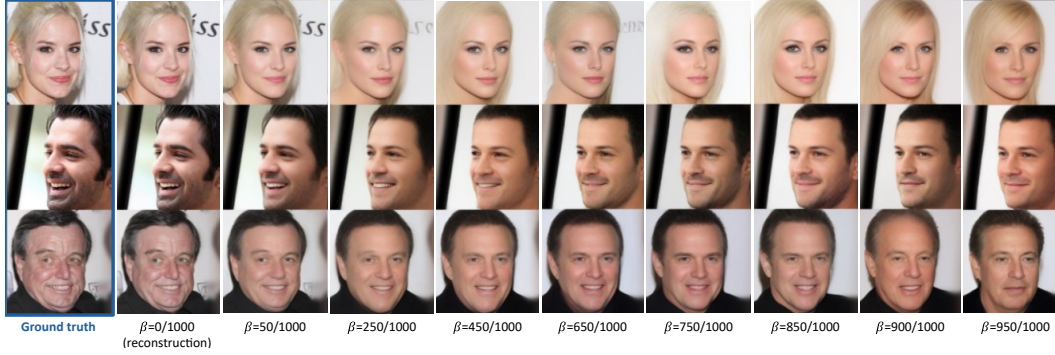


Figure 2: **Smoothness of latent space in $\beta(t)$:** We provide evidence for the smoothness of the learned representations by generating samples from latent spaces with various values of β . Notably, latent representations obtained by smaller β values tend to produce images closer to ground truth because they retain more information.

- Burgess, Christopher P., Irina Higgins, Arka Pal, Loic Matthey, Nick Watters, Guillaume Desjardins, and Alexander Lerchner (2017). “Understanding disentangling in β -VAE”. In: *Neural Information Processing Systems*.
- Chen, Ricky T. Q., Xuechen Li, Roger Grosse, and David Duvenaud (2018). “Isolating Sources of Disentanglement in Variational Autoencoders”. In: *Advances in Neural Information Processing Systems*.
- Collins, Jack H., Yifeng Huang, Simon Knapen, Benjamin Nachman, and Daniel Whiteson (Oct. 2022). “Machine-Learning Compression for Particle Physics Discoveries”. In: *Proc. International Conference on Learning Representation (ICLR)*.
- Dai, Bin and David Wipf (2019). “Diagnosing and enhancing VAE models”. In: *Proc. International Conference on Learning Representation (ICLR)*.
- Dewangan, Gaurav and Seetaram Maurya (2022). “Fault Diagnosis of Machines Using Deep Convolutional Beta-Variational Autoencoder”. In: *IEEE Transactions on Artificial Intelligence* 3.2, pp. 287–296.
- Dhariwal, Prafulla and Alexander Quinn Nichol (2021). “Diffusion Models Beat GANs on Image Synthesis”. In: *Advances in Neural Information Processing Systems*. Ed. by A. Beygelzimer, Y. Dauphin, P. Liang, and J. Wortman Vaughan.
- Eastwood, Cian and Christopher K. I. Williams (2018). “A framework for the quantitative evaluation of disentangled representations”. In: *International Conference on Learning Representations*.
- Esser, Patrick, Robin Rombach, Andreas Blattmann, and Björn Ommer (2021a). “ImageBART: Bidirectional Context with Multinomial Diffusion for Autoregressive Image Synthesis”. In: *Advances in Neural Information Processing Systems*. Ed. by A. Beygelzimer, Y. Dauphin, P. Liang, and J. Wortman Vaughan.
- Esser, Patrick, Robin Rombach, and Björn Ommer (June 2021b). “Taming Transformers for High-Resolution Image Synthesis”. In: *Proceedings of the IEEE/CVF Conference on Computer Vision and Pattern Recognition (CVPR)*, pp. 12873–12883.
- Fazlyab, Mahyar, Alexander Robey, Hamed Hassani, Manfred Morari, and George Pappas (2019). “Efficient and accurate estimation of lipschitz constants for deep neural networks”. In: *Proc. Advances in Neural Information Processing Systems (NeurIPS)*.
- Gondal, Muhammad Waleed, Manuel Wüthrich, Đorđe Miladinovic, Francesco Locatello, Martin Breidt, Valentin Volchkov, Joel Bessekun Akpo, Olivier Bachem, Bernhard Scholkopf, and Stefan Bauer (2019). “On the Transfer of Inductive Bias from Simulation to the Real World: a New Disentanglement Dataset”. In: *Neural Information Processing Systems*.
- He, Kaiming, Xiangyu Zhang, Shaoqing Ren, and Jian Sun (2016). “Deep Residual Learning for Image Recognition”. In: *2016 IEEE Conference on Computer Vision and Pattern Recognition (CVPR)*, pp. 770–778.
- Heusel, Martin, Hubert Ramsauer, Thomas Unterthiner, Bernhard Nessler, and Sepp Hochreiter (2017). “GANs Trained by a Two Time-Scale Update Rule Converge to a Local Nash Equilibrium”. In: *Advances in Neural Information Processing Systems*. Ed. by I. Guyon, U. Von Luxburg, S. Bengio, H. Wallach, R. Fergus, S. Vishwanathan, and R. Garnett. Vol. 30. Curran Associates, Inc.
- Higgins, Irina, Loic Matthey, Arka Pal, Christopher P. Burgess, Xavier Glorot, Matthew M. Botvinick, Shakir Mohamed, and Alexander Lerchner (2016). “beta-VAE: Learning Basic Visual Concepts

- with a Constrained Variational Framework”. In: *International Conference on Learning Representations*.
- Ho, Jonathan, Ajay Jain, and Pieter Abbeel (2020). “Denoising diffusion probabilistic models”. In: *Proceedings of the 34th International Conference on Neural Information Processing Systems*. NIPS ’20. Vancouver, BC, Canada: Curran Associates Inc.
- Hoffman, Matthew D and Matthew J Johnson (2016). “Elbo surgery: yet another way to carve up the variational evidence lower bound”. In: *Workshop in Advances in Approximate Bayesian Inference, NIPS*. Vol. 1. 2.
- Hooeboom, Emiel, Jonathan Heek, and Tim Salimans (23–29 Jul 2023). “simple diffusion: End-to-end diffusion for high resolution images”. In: *Proceedings of the 40th International Conference on Machine Learning*. Ed. by Andreas Krause, Emma Brunskill, Kyunghyun Cho, Barbara Engelhardt, Sivan Sabato, and Jonathan Scarlett. Vol. 202. Proceedings of Machine Learning Research. PMLR, pp. 13213–13232.
- Hooeboom, Emiel, Thomas Mensink, Jonathan Heek, Kay Lamerigts, Ruiqi Gao, and Tim Salimans (2024). *Simpler Diffusion (SiD2): 1.5 FID on ImageNet512 with pixel-space diffusion*.
- Karras, Tero, Timo Aila, Samuli Laine, and Jaakko Lehtinen (2018). “Progressive Growing of GANs for Improved Quality, Stability, and Variation”. In: *International Conference on Learning Representations*.
- Karras, Tero, Miika Aittala, Timo Aila, and Samuli Laine (2022). “Elucidating the Design Space of Diffusion-Based Generative Models”. In: *Proc. NeurIPS*.
- Karras, Tero, Miika Aittala, Jaakko Lehtinen, Janne Hellsten, Timo Aila, and Samuli Laine (2024). “Analyzing and Improving the Training Dynamics of Diffusion Models”. In: *Proc. CVPR*.
- Karras, Tero, Samuli Laine, and Timo Aila (2019). “A Style-Based Generator Architecture for Generative Adversarial Networks”. In: *2019 IEEE/CVF Conference on Computer Vision and Pattern Recognition (CVPR)*, pp. 4396–4405.
- Khrulkov, Valentin, Leyla Mirvakhabova, I. Oseledets, and Artem Babenko (2021). “Disentangled Representations from Non-Disentangled Models”. In: *ArXiv abs/2102.06204*.
- Kim, Dongjun, Seung-Jae Shin, Kyungwoo Song, Wanmo Kang, and Il-Chul Moon (2021). “Soft Truncation: A Universal Training Technique of Score-based Diffusion Model for High Precision Score Estimation”. In: *International Conference on Machine Learning*.
- Kim, Hyunjik and Andriy Mnih (2018). “Disentangling by Factorising”. In: *International Conference on Machine Learning*.
- Kingma, Diederik P. and Max Welling (2013). “Auto-Encoding Variational Bayes”. In: *CoRR abs/1312.6114*.
- Kynkäänniemi, Tuomas, Tero Karras, Samuli Laine, Jaakko Lehtinen, and Timo Aila (2019). “Improved Precision and Recall Metric for Assessing Generative Models”. In: *Neural Information Processing Systems*.
- Lin, Zinan, Kiran Thekumparampil, Giulia Fanti, and Sewoong Oh (13–18 Jul 2020). “InfoGAN-CR and ModelCentricity: Self-supervised Model Training and Selection for Disentangling GANs”. In: *Proceedings of the 37th International Conference on Machine Learning*. Ed. by Hal Daumé III and Aarti Singh. Vol. 119. Proceedings of Machine Learning Research. PMLR, pp. 6127–6139.
- Liu, Ziwei, Ping Luo, Xiaogang Wang, and Xiaoou Tang (2015). “Deep learning face attributes in the wild”. In: *Proceedings of the IEEE international conference on computer vision*, pp. 3730–3738.
- Locatello, Francesco, Stefan Bauer, Mario Lucic, Gunnar Raetsch, Sylvain Gelly, Bernhard Schölkopf, and Olivier Bachem (Sept. 2019). “Challenging Common Assumptions in the Unsupervised Learning of Disentangled Representations”. In: *Proceedings of the 36th International Conference on Machine Learning*. Ed. by Kamalika Chaudhuri and Ruslan Salakhutdinov. Vol. 97. Proceedings of Machine Learning Research. PMLR, pp. 4114–4124.
- Makhzani, Alireza, Jonathon Shlens, Navdeep Jaitly, and Ian J. Goodfellow (2015). “Adversarial Autoencoders”. In: *ArXiv abs/1511.05644*.
- Mathieu, Emile, Tom Rainforth, N. Siddharth, and Yee Whye Teh (2018). “Disentangling Disentanglement in Variational Autoencoders”. In: *International Conference on Machine Learning*.
- Parmar, Gaurav, Dacheng Li, Kwonjoon Lee, and Zhuowen Tu (June 2021). “Dual Contradistinctive Generative Autoencoder”. In: *Proceedings of the IEEE/CVF Conference on Computer Vision and Pattern Recognition (CVPR)*, pp. 823–832.
- Preechakul, Konpat, Nattanat Chatthee, Suttisak Wizadwongsa, and Supasorn Suwajanakorn (2022). “Diffusion autoencoders: Toward a meaningful and decodable representation”. In: *Proceedings of the IEEE/CVF conference on computer vision and pattern recognition*, pp. 10619–10629.

- Radford, Alec, Luke Metz, and Soumith Chintala (2015). “Unsupervised Representation Learning with Deep Convolutional Generative Adversarial Networks”. In: *CoRR* abs/1511.06434.
- Reed, Scott E, Yi Zhang, Yuting Zhang, and Honglak Lee (2015). “Deep Visual Analogy-Making”. In: *Advances in Neural Information Processing Systems*. Ed. by C. Cortes, N. Lawrence, D. Lee, M. Sugiyama, and R. Garnett. Vol. 28. Curran Associates, Inc.
- Ren, Xuanchi, Tao Yang, Yuwang Wang, and Wenjun Zeng (2022). “Learning Disentangled Representation by Exploiting Pretrained Generative Models: A Contrastive Learning View”. In: *ICLR*.
- Richards, Ryan J and Austen M Groener (2022). “Conditional β -VAE for de novo molecular generation”. In: *arXiv preprint arXiv:2205.01592*.
- Rombach, Robin, A. Blattmann, Dominik Lorenz, Patrick Esser, and Björn Ommer (2021). “High-Resolution Image Synthesis with Latent Diffusion Models”. In: *2022 IEEE/CVF Conference on Computer Vision and Pattern Recognition (CVPR)*, pp. 10674–10685.
- Sauer, Axel, Kashyap Chitta, Jens Müller, and Andreas Geiger (2021). “Projected GANs Converge Faster”. In: *Advances in Neural Information Processing Systems*. Ed. by M. Ranzato, A. Beygelzimer, Y. Dauphin, P.S. Liang, and J. Wortman Vaughan. Vol. 34. Curran Associates, Inc., pp. 17480–17492.
- Schonfeld, Edgar, Bernt Schiele, and Anna Khoreva (June 2020). “A U-Net Based Discriminator for Generative Adversarial Networks”. In: *Proceedings of the IEEE/CVF Conference on Computer Vision and Pattern Recognition (CVPR)*.
- Shao, Huajie, Shuochao Yao, Dachun Sun, Aston Zhang, Shengzhong Liu, Dongxin Liu, Jun Wang, and Tarek Abdelzaher (13–18 Jul 2020). “ControlVAE: Controllable Variational Autoencoder”. In: *Proceedings of the 37th International Conference on Machine Learning*. Ed. by Hal Daumé III and Aarti Singh. Vol. 119. Proceedings of Machine Learning Research. PMLR, pp. 8655–8664.
- Takida, Yuhta, Wei-Hsiang Liao, Chieh-Hsin Lai, Toshimitsu Uesaka, Shusuke Takahashi, and Yuki Mitsufuji (2022). “Preventing oversmoothing in VAE via generalized variance parameterization”. In: *Neurocomputing* 509, pp. 137–156.
- Vahdat, Arash, Karsten Kreis, and Jan Kautz (2021). “Score-based Generative Modeling in Latent Space”. In: *Advances in Neural Information Processing Systems*. Ed. by A. Beygelzimer, Y. Dauphin, P. Liang, and J. Wortman Vaughan.
- Wang, Yingheng, Yair Schiff, Aaron Gokaslan, Weishen Pan, Fei Wang, Christopher De Sa, and Volodymyr Kuleshov (2023a). “InfoDiffusion: representation learning using information maximizing diffusion models”. In: *Proceedings of the 40th International Conference on Machine Learning*. ICML’23. Honolulu, Hawaii, USA: JMLR.org.
- (2023b). “InfoDiffusion: representation learning using information maximizing diffusion models”. In: *Proceedings of the 40th International Conference on Machine Learning*. ICML’23. Honolulu, Hawaii, USA: JMLR.org.
- Wu, Qiucheng, Yujian Liu, Handong Zhao, Ajinkya Kale, Trung Bui, Tong Yu, Zhe Lin, Yang Zhang, and Shiyu Chang (2023). “Uncovering the disentanglement capability in text-to-image diffusion models”. In: *Proceedings of the IEEE/CVF conference on computer vision and pattern recognition*, pp. 1900–1910.
- Yang, Tao, Yuwang Wang, Yan Lu, and Nanning Zheng (2023). “DisDiff: Unsupervised Disentanglement of Diffusion Probabilistic Models”. In: *Thirty-seventh Conference on Neural Information Processing Systems*.
- Yeats, Eric, Frank Liu, David Womble, and Hai Li (2022). “NashAE: Disentangling representations through adversarial covariance minimization”. In: *European Conference on Computer Vision*. Springer, pp. 36–51.
- Yu, Fisher, Yinda Zhang, Shuran Song, Ari Seff, and Jianxiong Xiao (2015). “LSUN: Construction of a Large-scale Image Dataset using Deep Learning with Humans in the Loop”. In: *CoRR* abs/1506.03365.

Contents

1	Introduction	1
2	Overview of β-VAE	2
3	Multi-β Representation Learning	4
3.1	Conditional Multi-level β -VAE	4
3.2	Controlling Information Loss with β	4
4	Reversing the Information Loss	5
4.1	Primer on Diffusion Models	5
4.2	Non-linear Diffusion in Latent Space	6
5	Related Works	7
6	Experiments	8
6.1	Evaluating Disentanglement	8
6.1.1	Image Dataset	8
6.1.2	Common Benchmark with Toy Datasets	8
6.2	Evaluating Generation Quality	9
7	Conclusion	9
A	Supplementary for β-VAE	14
B	Proofs	14
B.1	Proposition 3.1	14
B.2	Proposition 3.2	15
C	Details of experiments	16
C.1	Details of Implementation	16
C.1.1	Disentanglement on Face Images	16
C.1.2	Disentanglement on Toy Experiments	16
C.1.3	Unconditional Image Generation	17
C.2	Latent manipulation and interpolation	19
D	Additional Results	19
D.1	Orthogonality of our method and DisCo	19
D.2	The relationship between β and disentanglement	19
D.3	Multi- β VAE Reconstructions	20
D.4	Generated Samples from Noise	20
D.5	Exploring the Spectrum of Learned Latents	23

A Supplementary for β -VAE

Disentanglement induced by larger β in β -VAE can be explained by breaking down the regularization term as outlined by Hoffman et al. (2016) and Makhzani et al. (2015):

$$\mathbb{E}_{p_{\mathcal{D}}(\mathbf{x})} [\text{D}_{\text{KL}}(q_{\phi}(\mathbf{z}|\mathbf{x})||p(\mathbf{z}))] = \mathcal{I}(\mathbf{z}; \mathbf{x}) + \text{D}_{\text{KL}}(q_{\phi}(\mathbf{z})||p(\mathbf{z})) \quad (20)$$

Here, $\mathcal{I}(\mathbf{z}; \mathbf{x})$ represents the mutual information between the latent variables and data points, and $q_{\phi}(\mathbf{z})$ is the marginal posterior distribution. Setting $\beta > 1$ forces $q_{\phi}(\mathbf{z})$ to be more similar to the factorized prior distribution, promoting independence within the latents. This also reduces the mutual information between the data and the latent variables, leading to information loss and poor reconstructions.

While the breakdown above explains why latent factors learned with $\beta > 1$ are more independent, it does not clarify why increasing the contribution of the *regularization term* leads to learning interpretable generative factors. In a dataset consisting of a variety of three-dimensional objects, these generative factors would include object type, orientation, scale, lighting, and color. Here, we subscribe to the hypothesis presented by Burgess et al. (2017) and Mathieu et al. (2018), which posits that by forcing the variational posterior $q_{\phi}(\mathbf{z}|\mathbf{x})$ to be more similar to the prior $p(\mathbf{z})$, we can achieve two desirable outcomes: (1) the scale of the prior forces the representations across data points to overlap, which inherently causes prominent generative attributes to overlap in the latent space; (2) the prior term also forces the variational posterior to be more factorized across data points, which results in different axes in \mathbf{z} corresponding to distinct generative factors.

B Proofs

B.1 Proposition 3.1

Formal restatement of Proposition 3.1 is provided as Proposition B.1 below.

Proposition B.1. *Assume that $p_{\mathcal{D}}(\mathbf{x})$ has finite covariance and f_{ϕ} is arbitrarily complex, provided it is Lipschitz continuous. For the global optimum of \mathcal{L}_{β} with respect to σ_{β}^2 , we have $\sigma_{\beta}^2 \rightarrow 0$ as $\beta \rightarrow 0$.*

The two assumptions in this proposition are reasonable in practice. Since $p_{\mathcal{D}}(\mathbf{x})$ is expressed as a sum of Dirac delta functions $\delta(\mathbf{x} - \mathbf{x}_i)$ for $i = 1, \dots, M$, where each \mathbf{x}_i represents a set of bounded pixel values, its covariance is finite. Furthermore, because f_{ϕ} is implemented within a deep neural network framework, it is expected to have strong representational capacity and to be Lipschitz continuous (Fazlyab et al., 2019). This proposition follows almost directly from Theorem 3 in Takida et al. (2022). For completeness, we provide the proof in this manuscript.

Proof. For a given β , consider the input sample \mathbf{x} and the reconstructed sample $\mathbf{x}' = g_{\theta}(\mathbf{z}_{\beta}, \beta)$ obtained via the stochastic latent variable $\mathbf{z}_{\beta} \sim q_{\phi}(\mathbf{z}_{\beta}|\mathbf{x}; \beta)$. Let \mathbf{z}_{β}^e denote the encoded latent variable without applying the reparameterization trick, i.e., $\mathbf{z}_{\beta}^e = f_{\phi}(\mathbf{x}, \beta)$. For improved readability, we omit β in probability distributions (e.g., $q_{\phi}(\mathbf{z}_{\beta}|\mathbf{x}; \beta)$). Define the marginalized distributions for \mathbf{z}_{β}^e and \mathbf{z}_{β} as $q_{\phi}(\mathbf{z}_{\beta}^e) := \mathbb{E}_{p_{\mathcal{D}}(\mathbf{x})}[\delta(\mathbf{z}_{\beta}^e - f_{\phi}(\mathbf{x}, \beta))]$ and $q_{\phi, \sigma_{\beta}^2}(\mathbf{z}_{\beta}) := \mathbb{E}_{p_{\mathcal{D}}(\mathbf{x})}[q_{\phi}(\mathbf{z}_{\beta}|\mathbf{x})]$, with their respective covariance matrices denoted as Σ_{ϕ}^e and $\Sigma_{\phi, \sigma_{\beta}^2}$. Additionally, let $q_{\sigma_{\beta}^2}(\mathbf{z}_{\beta}|\mathbf{z}_{\beta}^e)$ represent the conditional distribution of \mathbf{z}_{β} given \mathbf{z}_{β}^e .

By applying the data processing inequality to the Markov chain $\mathbf{x} \rightarrow \mathbf{z}_{\beta}^e \rightarrow \mathbf{z}_{\beta} \rightarrow \mathbf{x}'$, the following holds:

$$\mathcal{I}(\mathbf{z}_{\beta}, \mathbf{z}_{\beta}^e) \geq \mathcal{I}(\mathbf{x}, \mathbf{x}'). \quad (21)$$

Furthermore, the mutual information between \mathbf{z}_β and \mathbf{z}_β^e is bounded above as follows:

$$\mathcal{I}(\mathbf{z}_\beta, \mathbf{z}_\beta^e) = \mathcal{H}[q_{\phi, \sigma_\beta^2}(\mathbf{z}_\beta)] - \mathbb{E}_{q_\phi(\mathbf{z}_\beta^e)} \mathcal{H}[q_{\sigma_\beta^2}(\mathbf{z}_\beta | \mathbf{z}_\beta^e)] \quad (22)$$

$$\leq H(\Sigma_{\phi, \sigma_\beta^2}) - H(\sigma_\beta^2 \mathbf{I}) \quad (23)$$

$$= \frac{d}{2} \log \left(\frac{\det(\Sigma_{\phi, \sigma_\beta^2})}{\sigma_\beta^2} \right), \quad (24)$$

where $\mathcal{H}(p)$ and $H(\Sigma)$ denote the differential entropy of the distribution p and the Gaussian distribution with covariance Σ , respectively. By combining Equations (21) and (24), we arrive at the following:

$$\mathcal{I}(\mathbf{x}, \mathbf{x}') \leq \frac{d}{2} \log \left(\frac{\det(\Sigma_{\phi, \sigma_\beta^2})}{\sigma_\beta^2} \right). \quad (25)$$

To prove that $\sigma_\beta^2 \rightarrow 0$ as $\beta \rightarrow 0$, we show that (i) $\mathcal{I}(\mathbf{x}, \mathbf{x}')$, the LHS of Equation (25), diverges to positive infinity as $\beta \rightarrow 0$, and (ii) the determinant of Σ_{ϕ, σ^2} , appearing in the RHS, remains bounded above.

In relation to (i), we derive a lower bound for the mutual information as follows:

$$\begin{aligned} \mathcal{I}(\mathbf{x}, \mathbf{x}') &= \text{D}_{\text{KL}}(p_{\mathcal{D}}(\mathbf{x})p_{\theta, \phi}(\mathbf{x}' | \mathbf{x}) || p_{\mathcal{D}}(\mathbf{x})p_{\theta, \phi}(\mathbf{x}')) \\ &= \mathbb{E}_{p_{\mathcal{D}}(\mathbf{x})p_{\theta, \phi}(\mathbf{x}' | \mathbf{x})} [\log p_{\theta, \phi}(\mathbf{x}' | \mathbf{x}) - \log p_{\theta, \phi}(\mathbf{x}')] \\ &= \mathcal{H}[p_{\theta, \phi}(\mathbf{x}')] - \mathbb{E}_{p_{\mathcal{D}}(\mathbf{x})} \mathcal{H}[p_{\theta, \phi}(\mathbf{x}' | \mathbf{x})] \\ &\geq \mathcal{H}[p_{\theta, \phi}(\mathbf{x}')] - \mathbb{E}_{p_{\mathcal{D}}(\mathbf{x})} H(\beta \mathbf{I}), \end{aligned} \quad (26)$$

where $p_{\theta, \phi}(\mathbf{x}' | \mathbf{x}) := \mathbb{E}_{q_\phi(\mathbf{z} | \mathbf{x})} [p_\theta(\mathbf{x}' | \mathbf{z})]$ and $p_{\theta, \phi}(\mathbf{x}') := \mathbb{E}_{p_{\mathcal{D}}(\mathbf{x})} [p_{\theta, \phi}(\mathbf{x}' | \mathbf{x})]$. According to Theorem 4 in (Dai et al., 2019), we have $\mathcal{H}[p_{\theta, \phi}(\mathbf{x}')] \rightarrow \mathcal{H}[p_{\mathcal{D}}(\mathbf{x})]$ ($\beta \rightarrow 0$), and since $H(\beta \mathbf{I}) \rightarrow -\infty$ as $\beta \rightarrow 0$, it follows that $\mathcal{I}(\mathbf{x}, \mathbf{x}') \rightarrow \infty$ as $\beta \rightarrow 0$.

In relation to (ii), let V and L represent constants corresponding to the maximum singular value of the covariance of $p_{\mathcal{D}}(\mathbf{x})$ and Lipschitz constant of $f_\phi(\mathbf{x})$. Since the additive noise for the reparameterization trick follows a normal distribution $\mathcal{N}(0, \mathbf{I}_d)$, the covariance matrix satisfies $\Sigma_{\phi, \sigma^2} = \sigma^2 \mathbf{I} + \Sigma_\phi^e$. Therefore, we have

$$\det(\Sigma_{\phi, \sigma^2}) = \det(\sigma^2 \mathbf{I} + \Sigma_\phi^e) \leq (\sigma^2 + VL^2)^d < \infty, \quad (27)$$

where the upper bound is derived using the fact that the maximum singular value of Σ_ϕ^e is bounded above by VL^2 .

Finally, applying (i) and (ii) to Equation (25) conclude this proof. \square

B.2 Proposition 3.2

Proposition 3.2 The mutual information between the input and the reconstructed samples produced by the VAE becomes zero as $\text{D}_{\text{KL}}(q_\phi(\mathbf{z} | \mathbf{x}; \beta = 1) || p(\mathbf{z}))$ converges to zero. It holds for any decoder function $g_\theta(\cdot, \beta = 1)$.

This claim is almost direct consequence of Theorem 1 in Takida et al. (2022). For the sake of completeness, we provide the proof in this manuscript.

Proof. Let \mathbf{x} denote the input sample, with its corresponding latent variable represented as \mathbf{z} , and let \mathbf{x}' denote the reconstructed sample obtained via \mathbf{z} . These are defined as $\mathbf{z} \sim q_\phi(\mathbf{z} | \mathbf{x}; \beta = 1)$ and $\mathbf{x}' \sim p_\theta(\mathbf{x}' | \mathbf{z}; \beta = 1)$, respectively. Applying the data processing inequality to the Markov chain $\mathbf{x} \rightarrow \mathbf{z} \rightarrow \mathbf{x}'$ yields:

$$\mathcal{I}(\mathbf{x}; \mathbf{z}) \geq \mathcal{I}(\mathbf{x}; \mathbf{x}'), \quad (28)$$

Additionally, the mutual information $\mathcal{I}(\mathbf{x}; \mathbf{z})$ can be rewritten using its definition as follows:

$$\begin{aligned} \mathcal{I}(\mathbf{x}; \mathbf{z}) &= \text{D}_{\text{KL}}(p_{\mathcal{D}}(\mathbf{x})q_\phi(\mathbf{z} | \mathbf{x}) || p_{\mathcal{D}}(\mathbf{x})q_\phi(\mathbf{z})) \\ &= \mathbb{E}_{p_{\mathcal{D}}(\mathbf{x})q_\phi(\mathbf{z} | \mathbf{x})} [\log q_\phi(\mathbf{z} | \mathbf{x}) - \log q_\phi(\mathbf{z})] \\ &= \mathbb{E}_{p_{\mathcal{D}}(\mathbf{x})} \text{D}_{\text{KL}}(q_\phi(\mathbf{z} | \mathbf{x}) || p(\mathbf{z})) - \text{D}_{\text{KL}}(q_\phi(\mathbf{z}) || p(\mathbf{z})), \end{aligned} \quad (29)$$

where $p(\mathbf{z})$ denotes the prior distribution over \mathbf{z} . Since the Kullback-Leibler divergences $D_{\text{KL}}(q_\phi(\mathbf{z}|\mathbf{x})||p(\mathbf{z}))$ and $D_{\text{KL}}(q_\phi(\mathbf{z})||p(\mathbf{z}))$ are non-negative, it follows that:

$$\mathcal{I}(\mathbf{x}; \mathbf{z}) \leq \mathbb{E}_{p_{\mathcal{D}}(\mathbf{x})} D_{\text{KL}}(q_\phi(\mathbf{z}|\mathbf{x})||p(\mathbf{z})). \quad (30)$$

Combining inequalities (28) and (30) completes the proof. \square

C Details of experiments

C.1 Details of Implementation

We will open-source the Python code used to implement the method described in this work, along with the supporting scripts used for running the experiments. Our implementation is primarily based on the code provided by Rombach et al. (2021). For our method, we extend this existing codebase to implement our multi- β VAE (Section 3.1), the interpolating objective function based on a VAE’s ELBO objective (Eq. (4)), and the non-linear diffusion model (Section 4.2). Three Python files containing these core components of our implementation are included with our submission. A detailed list of the hyperparameters used in the experiments is provided below.

C.1.1 Disentanglement on Face Images

Table 4: Multi- β VAE architecture configuration for TAD measurement on CelebA.

Parameters	CelebA
Base channels	32
Channel multipliers	[1, 2, 4]
Attention resolutions	None
Number of res. blocks	2
Latent channels	4
Resolution	64
Input / Output channels	3 / 3
Dropout	0.0
Double \mathbf{z}	False
Embedding dim	4
Loss function	LPIPS + GAN + KL

Table 5: Non-linear Diffusion model architecture for TAD measurement on the CelebA dataset.

Parameters	CelebA
Base channels	64
Channel multipliers	[1, 2, 4, 4]
Attention resolutions	[1, 2, 4]
Attention heads	8
Model channels	64
β scheduler	Linear
$T = B$	1000

The architecture of our multi- β VAE and nonlinear diffusion model is designed to match that of Yang et al. (2023), with details presented in Table 4 and Table 5, respectively. For evaluation, we use the Total AUROC Difference metric and the code provided by Yeats et al. (2022).

C.1.2 Disentanglement on Toy Experiments

To ascertain the representations learned by our method in Section 6.1, we utilize small multi- β VAE architectures and employ the same convolutional backbone for implementing the baselines. Unlike previous works, we do not incorporate feed-forward layers in the architecture of the encoders and decoders. We assess the convergence of the model using the reconstruction loss.

For the architecture, all input images are resized to $64 \times 64 \times 3$, and we do not apply any data augmentation when training the multi- β VAE. For all methods presented in Table 2, we use a latent

dimensionality of 32. The encoder and decoder are symmetric networks that are fully convolutional. The encoder consists of four layers with [64, 64, 128, 256] channels, respectively, and we apply GroupNorm after every convolutional layer, followed by a Sigmoid non-linearity.

For training these models, we select a batch size of 150 and continue training until convergence is reached for each model. We used one NVIDIA L40S GPU for training on all these toy datasets. We trained our VAE with 500 values of β equally spaced within the range $[0, 1]$. We perform a sweep over all β values in our model to identify the optimal latent representation for each dataset. Specifically, for Cars3D, we achieve the highest score at $\beta = 285/500$; for Shapes3D, at $\beta = 210/500$; and for MPI3D, at $\beta = 280/500$. Table 2 demonstrates that our model achieves disentanglement performance comparable to or surpassing that of other disentanglement models.

C.1.3 Unconditional Image Generation

For architectures used in Section 6.2, we follow Rombach et al. (2021) and use architectures present in their code base. For all data sets, we used an image resolution of 256×256 and compress the input by a factor of 8 leading to a latent dimensionality of $32 \times 32 \times 4$. We fix the multi- β VAE architecture across datasets with the encoder and decoder each containing 4 layers, each comprising 2 ResNet (He et al., 2016) blocks with [128, 256, 512, 768] channels, respectively.

Algorithm 3: Forward Pass for ResNet Block with Time Embedding

Input: Input x , Temporal embedding $temb$

Output: Output h

```

 $h \leftarrow x$ 
 $h \leftarrow \text{GroupNorm}(h)$ 
 $h \leftarrow \text{Sigmoid}(h)$ 
 $h \leftarrow \text{Conv}(h)$ 
 $h \leftarrow h + \text{Proj}(\text{Sigmoid}(temb))$ 
 $h \leftarrow \text{GroupNorm}(h)$ 
 $h \leftarrow \text{Sigmoid}(h)$ 
 $h \leftarrow \text{Dropout}(h)$ 
 $h \leftarrow \text{Conv}(h)$ 
return  $x + h$ 

```

We present a simplified version of the ResNet block we use in Algorithm 3. We use attention at a resolution of 16×16 and the encoder and decoder are symmetric. The total number of trainable parameters on the multilevel β -VAE is 148 Million.

For implementing the non-linear diffusion model (Section 4.2), we increase the U-Net’s output channels to 8 and leave the rest of the architecture unmodified. As our diffusion model produces two outputs and is designed to model the noise at every time step along with a difference predictor (Eq. (17)) we use more than 300 Million parameters in our testing and report results with a network having 378 Million trainable parameters. Table 6 lists the hyperparameters we used for training the unconditional diffusion models for all data sets. Next, we elaborate on the learned noise schedules.

Noise Schedule: As elaborated in Section 3.2 our method learns σ_β as a result of training the multi- β VAE which is the first stage of training irrespective of the dataset. The σ_β obtained at the termination of this first stage of training is dependent on the choice of schedules of β which control the coefficients of *reconstruction term* and *regularisation term* in Eq. (4). In the following plot, we present two examples of learned noise schedules using empirically determined β schedules and contrast it with a linear noise schedule.

The training of the non-linear diffusion model is sensitive to the setting of this schedule, for instance, none of our models work well for a schedule that grows sub-linearly for $t < 0.5$. The sudden increment in noise close to $\beta = 0$ does not affect the model’s performance negatively. Such a sigma schedule is obtained by following a sinusoidal schedule for β . The exact form of our schedule is present in the shared code.

Table 6: Hyperparameters for the unconditional LDMs producing the numbers shown in Table 3. All models trained on 4 NVIDIA H100 GPUs.

	CelebA-HQ 256×256	FFHQ 256×256	LSUN-Bedrooms 256×256
f	4	4	4
z -shape	$32 \times 32 \times 4$	$32 \times 32 \times 4$	$32 \times 32 \times 4$
Diffusion steps	1000	1000	1000
$\mathcal{N}_{\text{params}}$	378M	378M	378M
Channels	256	256	256
Depth	2	2	2
Channel Multiplier	1,3,5	1,3,5	1,3,5
Attention resolutions	32, 16, 8	32, 16, 8	32, 16, 8
Head Channels	32	32	32
Batch Size	98	98	98
Iterations*	120k	180k	300k
Learning Rate	5.6e-5	4.4e-5	4.4e-5

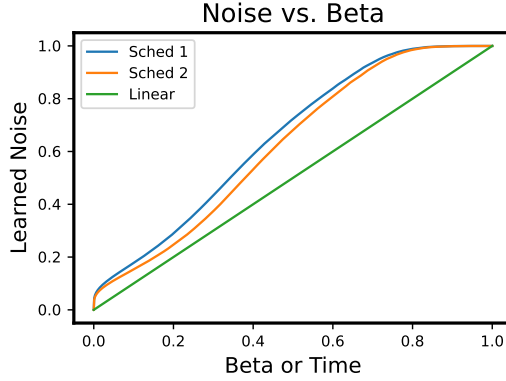


Figure 3: Examples of preferable noise schedules in our framework. These noise schedules have been used for learning non-linear diffusion models in Table 3. While CelebAHQ (Karras et al., 2018) trains better with Sched 1, both FFHQ (Karras et al., 2019) and LSUN-Bedrooms (Yu et al., 2015) train better with Sched 2.

C.2 Latent manipulation and interpolation

Algorithm 4: Manipulate images with given direction

Input : Multi- β VAE (θ, ϕ) , Non-linear diffusion model $(\epsilon_\psi, \Delta_\psi)$, an image \mathbf{x} , latent direction δ , manipulation factor α , time step $t = \beta$

Output : Manipulated image \mathbf{x}_{man}

```

1   Encode the image as  $\mathbf{z}_\beta = f_\phi(\mathbf{x}, \beta)$ 
2   Add the perturbation to the encoded latent  $\tilde{\mathbf{z}}_\beta = \mathbf{z}_\beta + \alpha\delta$ 
3   Denoise  $\tilde{\mathbf{z}}_\beta$  back to  $\beta = 0$  using diffusion model  $(\epsilon_\psi, \Delta_\psi)$ 
4   Decode  $\tilde{\mathbf{z}}_0$  as  $\mathbf{x}_{\text{man}} = g_\theta(\tilde{\mathbf{z}}_0, \beta = 0)$ 
5   return  $\mathbf{x}_{\text{man}}$ 

```

Algorithm 5: Interpolate a pair of images

Input : Multi- β VAE (θ, ϕ) , Non-linear diffusion model $(\epsilon_\psi, \Delta_\psi)$, images \mathbf{x}_1 and \mathbf{x}_2 , interpolation factor α , target dimensions to interpolate Λ , time step $t = \beta$

Output : Interpolated image \mathbf{x}_{int}

```

1   Encode the images as  $\mathbf{z}_{\beta,1} = f_\phi(\mathbf{x}_1, \beta)$  and  $\mathbf{z}_{\beta,2} = f_\phi(\mathbf{x}_2, \beta)$ 
2   Initialize the latent variable as  $\tilde{\mathbf{z}}_\beta = \mathbf{z}_{\beta,1}$ 
3   Interpolate latent variables as  $\tilde{\mathbf{z}}_\beta[j] = \text{Slerp}(\mathbf{z}_{\beta,1}[j], \mathbf{z}_{\beta,2}[j], \alpha)$  for  $j \in \Lambda$ 
4   Denoise  $\tilde{\mathbf{z}}_\beta$  back to  $\beta = 0$  using diffusion model  $(\epsilon_\psi, \Delta_\psi)$ 
5   Decode  $\tilde{\mathbf{z}}_0$  as  $\mathbf{x}_{\text{int}} = g_\theta(\tilde{\mathbf{z}}_0, \beta = 0)$ 
6   return  $\mathbf{x}_{\text{int}}$ 

```

In Fig. 1, we obtain high-fidelity manipulated images by following Algorithm 4. The candidates for the latent direction δ are eigenvectors obtained via Principal Component Analysis (PCA) of a large set of latent embeddings. Algorithm 5 presents the pseudocode for interpolating between two images, with examples of the interpolated images shown in Fig. 7. We begin by producing an interpolated encoding at a time step t using an interpolation coefficient α to control the mixing between \mathbf{z}_1 and \mathbf{z}_2 . Both algorithms require a trained multi- β VAE and the corresponding nonlinear diffusion model to generate high-fidelity images.

D Additional Results

This section presents additional results from applying our method to high-quality image datasets. In Appendix D.1, we demonstrate that our approach is complementary to learning-free methods by comparing it with DisCo (Ren et al., 2022). In Appendix D.2, we investigate the relationship between disentanglement and the value of β . In Appendix D.3, we show additional reconstructions generated by the multi- β VAE. Appendix D.4 includes samples generated by our model for qualitative evaluation, supporting the results presented in Table 3 and confirming that our model can function as a standalone generative model. Furthermore, Appendix D.5 explores the spectrum of learned latent representations through latent interpolation and attribute editing.

D.1 Orthogonality of our method and DisCo

In this subsection, we follow the same experimental setup as Section 6.1.2. As shown in Table 7, our multi- β VAE achieves better disentanglement performance compared to DisCo applied to standard VAE. Furthermore, DisCo consistently performs best when applied to multi- β VAE, indicating that DisCo and our approach are complementary. Notably, while DisCo significantly improves standard VAE’s performance, its impact on multi- β VAE is relatively marginal, suggesting that our model’s latent space is already well-disentangled.

D.2 The relationship between β and disentanglement

To further investigate the properties of latent representations learned at different β values, we plot the evolution of the MIG score as a function of β using the Cars3d dataset. These results are presented in Fig. 4. The plot reveals that MIG scores fluctuate in alignment with the loss function (4) associated

Table 7: Disentanglement results. The experimental setup follows Section 6.1, using identical VAE architectures for all methods.

	Metrics	VAE	DisCo on VAE	Multi- β VAE	DisCo on Multi- β VAE
Cars	MIG (\uparrow)	0.037 ± 0.022	0.071 ± 0.029	0.114 ± 0.009	0.116 ± 0.011
	DCI (\uparrow)	0.063 ± 0.037	0.127 ± 0.044	0.157 ± 0.010	0.171 ± 0.010
Shps	MIG (\uparrow)	0.167 ± 0.112	0.237 ± 0.134	0.422 ± 0.090	0.434 ± 0.090
	DCI (\uparrow)	0.363 ± 0.027	0.526 ± 0.045	0.621 ± 0.090	0.678 ± 0.081
MPI	MIG (\uparrow)	0.021 ± 0.013	0.047 ± 0.027	0.147 ± 0.035	0.152 ± 0.029
	DCI (\uparrow)	0.096 ± 0.024	0.188 ± 0.042	0.253 ± 0.043	0.284 ± 0.060

with each β value. For models like β -TCVAE, β -VAE, and FactorVAE, determining an optimal coefficient for regularization can be challenging, often requiring numerous training runs as the ideal coefficient depends on both the dataset and model architecture. In our approach, this issue is mitigated by training a conditional β model across a wide range of β values (Section 3.1). Building on this analysis, we highlight an additional insight gained from using multiple β values. By leveraging the distinct generative factors in the toy datasets, we plotted the highest mutual information for two factors across all β values, showing that while mutual information (MI) increases for ‘Pitch’ as β increases, it decreases for ‘Identity’ (see Fig. 4). This observation supports the idea of training a model across multiple β values, as it enables targeted manipulation of image factors by selecting specific β values.

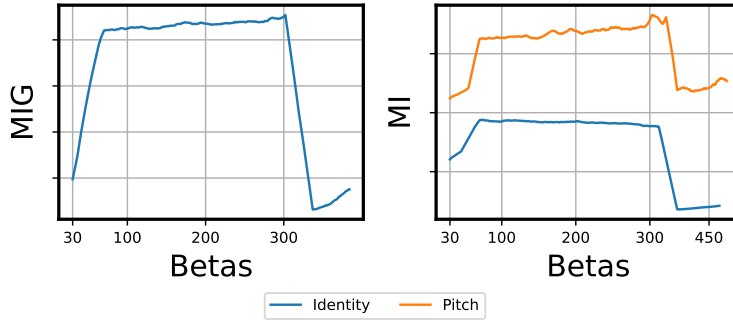


Figure 4: **Variation of MIG and MI:** We analyze the variation in MIG and MI scores of generative factors across different β values on the Cars3D dataset (Reed et al., 2015) to quantitatively track disentanglement in the latent space. Notably, the highest MIG scores for each factor are achieved at different β values.

D.3 Multi- β VAE Reconstructions

Fig. 5 shows reconstructions generated solely by our multi- β VAE on the image datasets. To create these images, the same value of β is passed to both the encoder and decoder networks. The figure displays a range of β values, demonstrating that the latent representation loses information about the input image as β increases. We would like to emphasize again that our non-linear diffusion model can generate additional information and decode the latent representation into high-fidelity images at any β values, as shown in Fig. 2.

D.4 Generated Samples from Noise

In Fig. 6, we show samples generated by our method, which combines a multi- β VAE with a non-linear diffusion model, on the image datasets listed in Table 3. To generate samples, we begin by sampling a batch of noise from a standard normal distribution and then apply Algorithm 2 to denoise it to $\beta = 0$. In the final step, we decode the denoised latent sample into the pixel space using the trained decoder as $\mathbf{x} = g_\theta(\mathbf{z}_0, \beta = 0)$. We train our non-linear diffusion models for 1000 steps (refer to Table 6) and thus sample for 1000 steps.

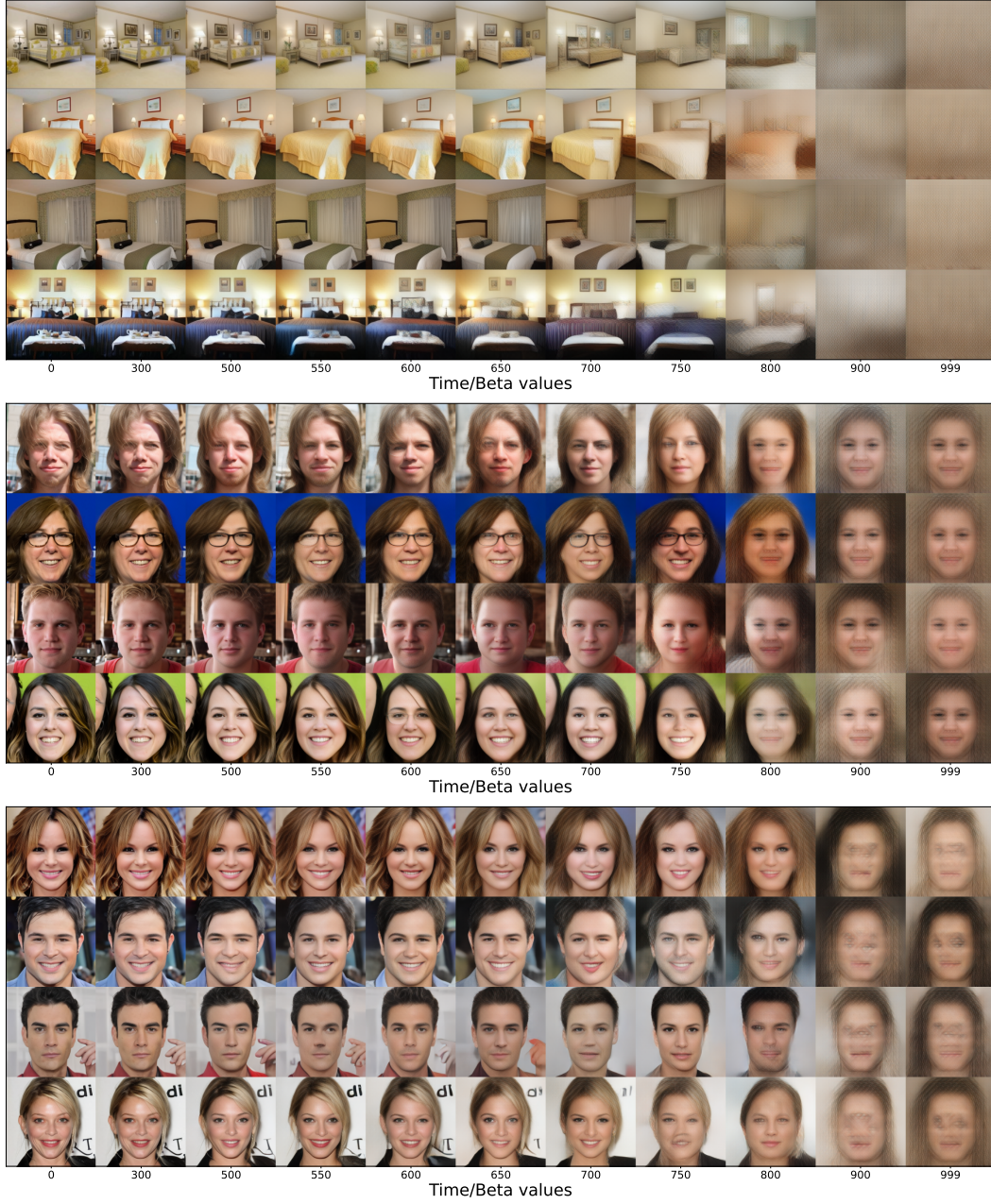


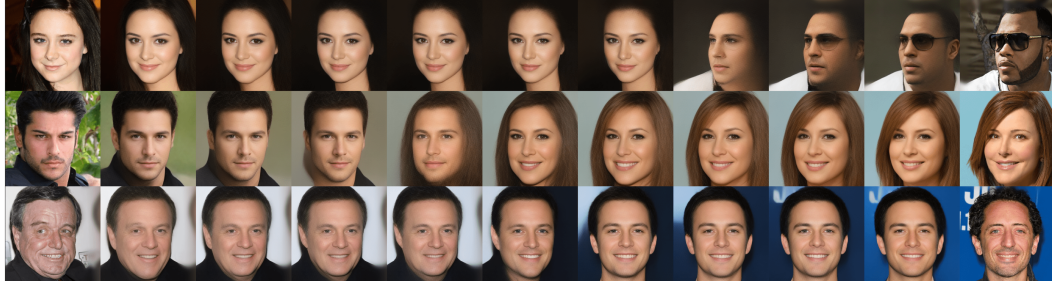
Figure 5: This figure presents examples of how our multi- β VAE reconstructs images across different datasets as β is varied. The top panel shows reconstructions on LSUN-Bedrooms (Yu et al., 2015), the middle panel displays FFHQ (Karras et al., 2019) reconstructions, and the bottom panel contains CelebA-HQ (Karras et al., 2018) reconstructions. Please refer to Fig. 2 for reconstructed images through multi- β VAE and non-linear diffusion model.



Figure 6: Samples generated by models trained on CelebA-HQ (Karras et al., 2018) (top), FFHQ (Karras et al., 2019) (middle), and LSUN-Bedrooms (Yu et al., 2015) (bottom). These samples demonstrate that our model can function as a standalone generative model.



(a) $\beta = 0/1000$



(b) $\beta = 300/1000$



(c) $\beta = 600/1000$



(d) $\beta = 900/1000$

Figure 7: **Interpolation in latent space:** We interpolate pairs of images (shown in the leftmost and rightmost columns) by applying slerp to the latent spaces.

D.5 Exploring the Spectrum of Learned Latents

We investigate the properties of latent spaces by interpolating pairs of images using spherical linear interpolation (slerp), as shown in Fig. 7. We selected four values for β to explore how the β value affects the interpolated images. The latent space with the smallest value, $\beta = 0$, is not regularized by the KL term, resulting in continuous but meaningless interpolation. As we gradually increase the value of β , the interpolated images transition more smoothly in the meaningful pixel space. Larger values of β yield more natural-looking face images, although this comes at the cost of continuity in the image transitions. It is worth noting that even with large β values, such as $\beta = 900/1000$, the resulting images maintain high fidelity, which is a distinct property compared to traditional β -VAE.

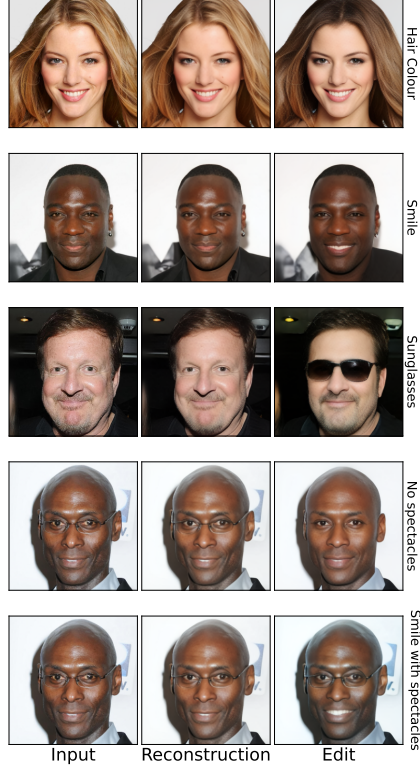


Figure 8: This figure contains more examples of editing of facial attributes of a person. In the first row we modify hair colour, in the second row we add a smile, in the third row we add sunglasses, in the fourth row we remove spectacles and in the final row we keep the spectacles while adding a smile. We source these input images from the CelebA-HQ (Karras et al., 2018) and FFHQ (Karras et al., 2019) datasets.

Additionally, we show examples of attribute changes in Fig. 8. We follow Algorithm 4 to obtain the manipulated images.

E Limitations and Broader Impacts

Limitations. Our model is trained in a completely unsupervised manner. While this approach allows us to learn disentangled representations without the need for labeled data, it necessitates the use of additional tools, such as PCA, to edit input images as desired, as demonstrated in the appendix. Although our primary focus is on developing generative models that can learn disentangled representations and perform downstream tasks without relying on extra conditioning, we recognize that incorporating text conditioning capabilities into our method could lead to more interpretable representations. This is a promising direction for future work. Furthermore, our sampling method for the non-linear diffusion model is similar to DDPM rather than DDIM. Consequently, developing a DDIM-based sampling method for faster generation remains an area for future exploration. Lastly, non-linear diffusion model is still a relatively unexplored area compared to linear diffusion models. While our model demonstrates promising results, we anticipate that future research focused on non-linear diffusion model could further enhance generation quality and expand the capabilities of generative models.

Broader Impacts. As with any general image generation model, our approach carries the risk of producing harmful or inappropriate content, which is contingent upon the datasets used for training. We have utilized image datasets that have been widely accepted for academic purposes. However, it is essential to acknowledge that even well-curated datasets may contain biases or reflect societal stereotypes, which can inadvertently influence the outputs of our model.